Available online at www.sciencedirect.com

jmr&t Journal of Materials Research and Technology

www.jmrt.com.br

Original Article

Automatic characterization of iron ore by digital microscopy and image analysis☆

Julio César Álvarez Iglesias[a], *Karen Soares Augusto*[a], *Otávio da Fonseca Martins Gomes*[b,c,*], *Alei Leite Alcântara Domingues*[d], *Maria Beatriz Vieira*[d], *Catia Casagrande*[e], *Sidnei Paciornik*[a]

[a] *Department of Chemical and Materials Engineering, PUC-Rio, Rua Marquês de São Vicente, 225, Rio de Janeiro 22451-900, Brazil*

[b] *Centre for Mineral Technology (CETEM), Av. Pedro Calmon, 900, Ilha da Cidade Universitária, 21941-908 Rio de Janeiro, Brazil*

[c] *Postgraduate Program in Geosciences, National Museum, UFRJ, Av. Quinta da Boa Vista, S/N, São Cristóvão, 20940-040 Rio de Janeiro, Brazil*

[d] *Ferrous Technology Center (CTF), Vale, Centro de Pesquisas do Miguelão, Av. de Ligação 3580, Nova Lima, 34000-000 Minas Gerais, Brazil*

[e] *Pelletizing Direction (DIPE), Vale, Complexo de Tubarão, Avenida Dante Michelini, 5500, 29090-900 Vitória, Espírito Santo, Brazil*

ARTICLE INFO

Article history:
Received 19 November 2017
Accepted 10 June 2018
Available online 1 August 2018

Keywords:
Iron ore
Texture
Characterization
Image analysis
Classification

ABSTRACT

This paper presents an automatic system for mineralogical and textural characterization of iron ores based on digital microscopy and image analysis. It employs a motorized and computer-controlled reflected light microscope in a correlative approach that combines bright field and circular polarization modes. Mosaic images covering large areas of polished sections are acquired to image thousands of particles. Different classifiers discriminate compact and non-compact hematite, polycrystalline and monocrystalline particles, and identify particles as granular, lamellar, and lobular. The entire process is automatic and produces a full pdf report containing typical images and the quantification of mineral and textural phases.

1. Introduction

Microstructural characterization has been increasingly recognized as an important tool since it provides mineralogical and textural information that can improve iron ore beneficiation operations and subsequent steelmaking processes. Therefore, the industry is moving from the qualitative evaluation on the optical microscope toward quantitative and automatic methods based on digital microscopy and image analysis. In the last decade, several such methods were developed [1–10].

☆ Paper was part of technical contributions presented in the events part of the ABM Week 2017, October 2nd to 6th, 2017, São Paulo, SP, Brazil.

* *Corresponding author.*
E-mail: ogomes@gmail.com (O. da Fonseca Martins Gomes).

https://doi.org/10.1016/j.jmrt.2018.06.014

Automatic image analysis systems can easily recognize the most common iron-bearing minerals (hematite, magnetite and goethite) by their characteristic colors on suitable images acquired on a reflected light microscope (RLM) in bright field (BF) mode. On the other hand, the use of crossed polarizers in the RLM makes the crystals of hematite present different brightness and colors according to their crystalline orientation, revealing the hematite textures. Pirard et al. [2] and Iglesias et al. [6] proposed methods that use crossed linear polarizers in multiple angles and BF images to analyze hematite crystals. Gomes et al. [7] developed a method to identify and classify individual hematite crystals according to Vale's textural typology of hematite using BF and circularly polarized light (CPOL) modes. This latter method presented good results, but it is limited to the three compact classes (granular, lamellar and lobular), it cannot identify or classify the non-compact microcrystalline and martite classes.

The present paper describes the current state of complete system for iron ore characterization developed in a collaboration between PUC-Rio and Vale. The system is fully automatic comprising image acquisition in both BF and CPOL modes, identification and quantification of mineral and textural phases, recognition and quantification of polycrystalline and monocrystalline particles.

2. Materials and methods

2.1. *Sample preparation*

Samples of iron ore fines (pellet feed), provided by Vale, were embedded in epoxy resin to form blocks with 30 mm of diameter. The blocks were ground using diamond impregnated metal discs with 70 μm sized diamond particles, followed by particle sizes 40, 15 and 6 μm. This grinding was carried out with water for 2 min for the first three particle sizes and 4 min for the last one. After grinding, the blocks underwent an ultrasonic bath to remove any possible residues, to prevent scratching during polishing. The polishing procedure used cloths with diamond suspensions of 3 and 1 μm for approximately 1 h each, generating highly polished sections.

2.2. *Image acquisition and mosaicing*

The system is assembled with a motorized and computer-controlled reflected light microscope Zeiss Axioimager M2.m with a digital camera Zeiss Axiocam MRc5 (up to 2584 × 1936 pixels of resolution). A routine implemented in the AxioVision 4.9.1 software controls the microscope and performs automatic image acquisition and mosaicing. The operator just needs to set the polished section in the microscope stage, set the mosaic size, and adjust acquisition conditions (illumination, filters, camera parameters, etc.) with previously values defined. Thus, several images, in both BF and CPOL modes, are acquired to compose mosaic images covering representative areas of the sample.

In CPOL mode, instead of acquiring conventional full field images, the current version of the system acquires centered subframes with 200 × 200 pixels. This procedure takes advantage of the more homogenous illumination in the center of field, avoiding the background correction step that worsens the contrast between hematite crystals and consequently impairs their segmentation [8]. The use of subframe acquisition increases the acquisition time, but this problem is minimized with routine automation.

In the present case-study, all images were obtained with the 20× objective lens (EC Epiplan 20X/0.40) in 24 bits RGB color quantization with a spatial resolution of 0.53 μm/pixel. The BF and CPOL mosaics were respectively composed by 6 × 3 full frame images (1292 × 968 pixels) and 49 × 25 subframes images (200 × 200 pixels).

2.3. *Image processing and analysis*

All the image processing and analysis steps were performed in Fiji/ImageJ [11] and Octave [12] open source environments. A routine implemented in Scheme programming language [13] integrates them and provides a multicore parallel processing to speed up the analysis. The image processing and analysis steps are described in the following section together with results.

3. Results

BF and CPOL mosaic images present a small displacement between them. It occurs due to subframe acquisition procedure that produces a mosaic with different size and because polarizers are mounted slightly oblique to the optical axis to avoid spurious reflections in the microscope. Thus, before any further processing, each pair of mosaic images was registered using the Fiji plugin Linear Stack Alignment with SIFT [14].

Fig. 1 presents the image analysis flowchart. The identification and segmentation of iron-bearing phases (hematite, magnetite and goethite) were carried out by intensity thresholding of the BF mosaic image with pre-defined fixed thresholds. In practice, it automates the segmentation of those phases because they present distinct gray levels that remain constant if the acquisition conditions are kept stable. This reproducibility is precisely one of the advantages of using automatic acquisition as opposed to the human operator.

Fig. 2 shows the input BF image (Fig. 2a) and some resulting images (Fig. 2b–h). It is worth mentioning that these images represent a small region of the mosaics, because their full size would prevent the finer structures from being observed in detail.

Hematite, magnetite and goethite segmented regions can be seen in Fig. 2b painted with false colors (hematite in cyan, magnetite in yellow and goethite in magenta). In this field the magnetite has a fraction of 1%, and is not visible. Magnetite and goethite go on directly to the 'Measurement' step while the hematite feeds the 'Synthetic Method'. This step uses the segmented hematite image as a mask to remove any pixel outside the hematite phase in the CPOL image (Fig. 2c) and subsequently discriminates non-compact (Fig. 2d) and compact hematite (Fig. 2e) through supervised classification using textural features. It is used the quadratic classifier available in the Octave environment trained with a set of images previously classified by an expert from Vale and with overall success rate above 90%. The textural features employed

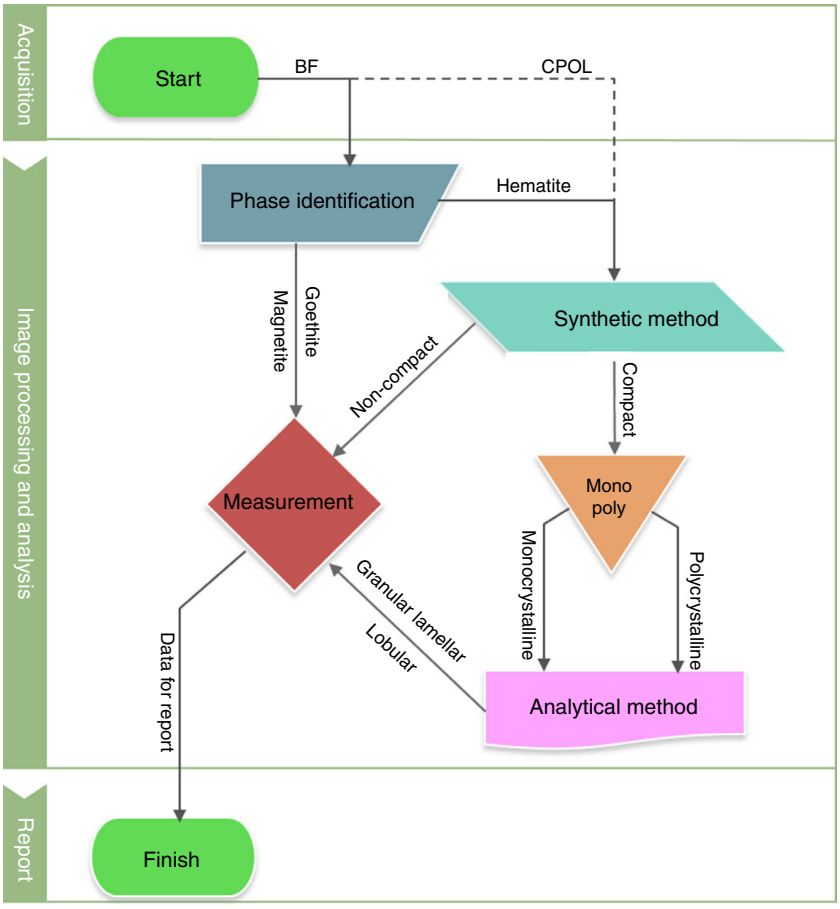

Fig. 1 – Image analysis flowchart.

are based on the so-called Haralick parameters [15] that were originally proposed for distinguishing different kinds of terrain in remote sensing applications. They represent several statistics of the co-occurrence of pixel intensities. Differently from typical occurrence statistics, the co-occurrence statistics computes the probability of pairs of pixel values at different distances and orientations. In our system, the first neighbors in an 8-neighborhood are considered, and, since directional characteristics are not important for this classification, the average and the range of each of the eleven first Haralick parameters computed at all orientations are employed.

Non-compact hematite goes on then to 'Measurement', while compact hematite follows to the 'Mono-Poly Separation' step. As its name suggests, this step separates monocrystalline (Fig. 2f) and polycrystalline (Fig. 2g) hematite particles. It is carried out through supervised classification using textural and morphological features and the quadratic classifier of Octave with success rate above 90%. The textural features employed are the entropy and the coefficient of variation of intensities. The morphological feature is the ratio of perimeters measured after the application of the Canny edge detector [16] to the image of hematite and to the CPOL image masked by hematite (Fig. 2c). The hematite image denotes the particles, and the CPOL image displays the crystals. Monocrystalline particles present this perimeter ratio very close to 1, and it tends to be smaller the more crystals the particle has. Following, monocrystalline and polycrystalline hematite particles feed the 'Analytical Method' [7], which classifies them into granular, lamellar or lobular (Fig. 2h), and, then, they go to 'Measurements'.

The quantification results are presented by three plots of area fraction: mineral phases plus martite (Fig. 3a); monocrystalline versus polycrystalline hematite particles (Fig. 3b); and the three types of compact hematite (Fig. 3c).

The mineral phases (hematite, magnetite and goethite) are measured from the image resulting from the 'Phase Identification' step (Fig. 2b). However, martite cannot be identified at this step since it can be composed by hematite and magnetite. Thus, martite is measured from the image resulting from the 'Synthetic Method'. It is worth noting that in the case of this sample, it is not necessary to discriminate martite and microcrystalline hematite from non-compact hematite, since it does not contain microcrystalline hematite. Thus, all non-compact hematite can be counted as martite (Fig. 2d). If martite and microcrystalline hematite were present, the output of the 'Synthetic Method' would be a false color image discriminating them.

The system integrates the creation of an automatic pdf report containing typical images and the quantification results, programmed in the LaTeX language [17].

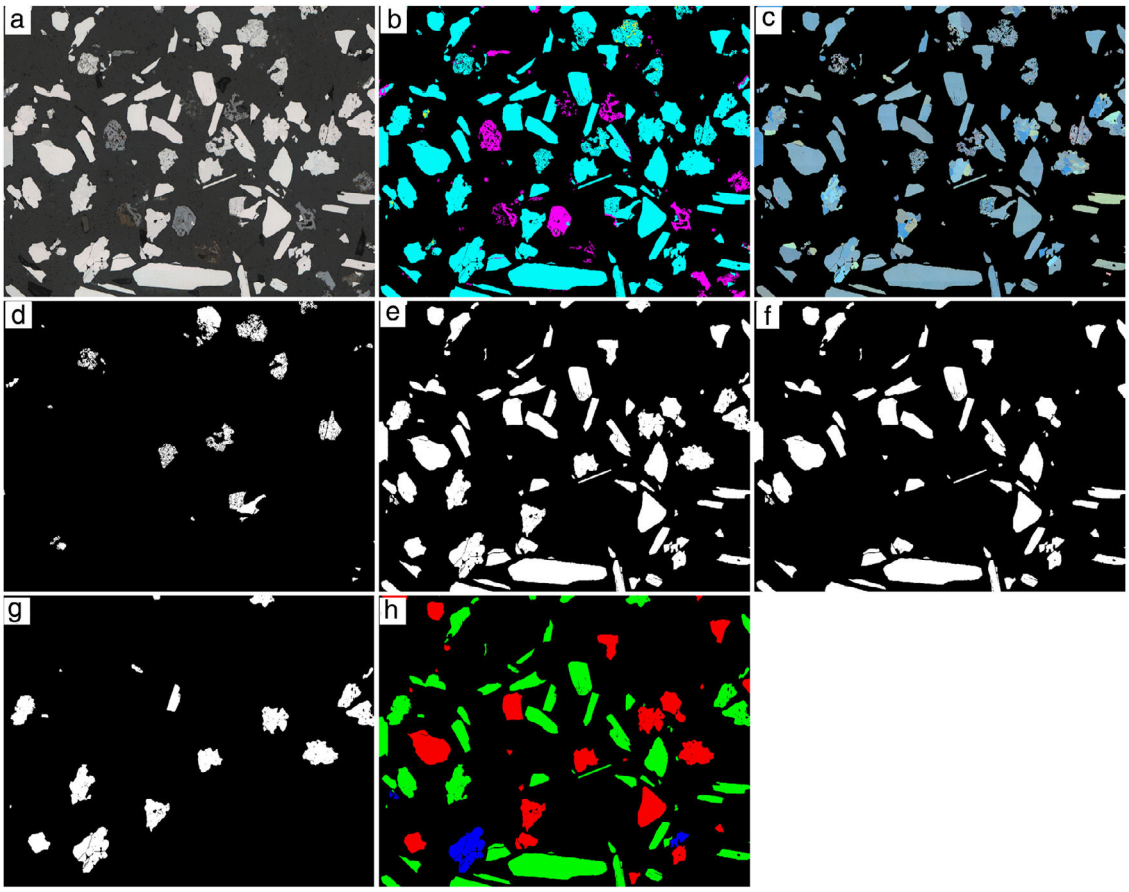

Fig. 2 – Input and resulting images: (a) BF image; (b) mineralogical phases – hematite in cyan, magnetite in yellow and goethite in magenta; (c) CPOL Image masked by hematite segmented from BF image; (d) non-compact hematite; (e) compact hematite; (f) monocrystalline particles; (g) polycrystalline particles and (h) types of compact hematite – granular in red, lamellar in green and lobular in blue.

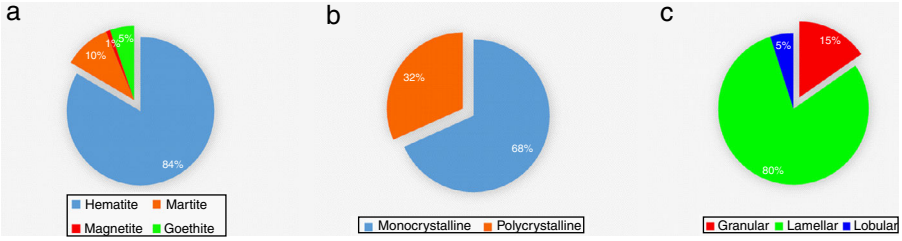

Fig. 3 – Area fraction of (a) mineralogical phases; (b) mono and polycrystalline hematite particles; and (c) compact hematite types.

4. Conclusion

The development of the system and its gradual implementation over the years in Vale's laboratories indicate the viability of fully automating procedures for iron ore characterization based on reflected light microscopy. The combination of motorized optical microscopy with integrated image acquisition in different contrast modes (BF and CPOL), and automatic segmentation and classification routines built an analytical solution for iron ore fines that is operator independent, reducing time consumption and improving the reproducibility of results. The classification algorithms should evolve with the continued use of the system, increasing their success rates, which is already competitive with the human recognition capacity. Modern artificial intelligence techniques such as deep learning neural networks may, in the future, improve the classification steps. Ultimately, the daily use of the system by Vale teams will allow its validation and refinement, and the application of the same concepts to other ore characterization issues.

Conflicts of interest

The authors declare no conflicts of interest.

Acknowledgements

The authors thank Vale for the material provided for this work, and CNPq and FAPERJ, Brazilian agencies, for the financial support.

REFERENCES

[1] Donskoi E, Suthers SP, Fradd SB, Young JM, Campbell JJ, Raynlyn TD, et al. Utilization of optical image analysis and automatic texture classification for iron ore particle characterization. Miner Eng 2007;20:461–71.
[2] Pirard E, Lebichot S, Krier W. Particle texture analysis using polarized light imaging and grey level intercepts. Int J Miner Process 2007;84:299–309.
[3] Gomes ODM, Paciornik S. Iron ore quantitative characterization through reflected light-scanning electron co-site microscopy. In: The AusIMM organizer. Proceedings of the 9th international congress on applied mineralogy. 2008. p. 699–702.
[4] Wagner DT, Rouco HV, Gomes ODM, Paciornik S, Vieira MB. Iron ore pellet characterization through digital microscopy. In: ABM organizer. Annals of 2nd international symposium on iron ore. 2008. p. 231–6.
[5] Gomes ODM, Paciornik S, Iglesias JCA. A simple methodology for identifying hematite grains under polarized reflected light microscopy. In: CI/UFF organizer. Proceedings of the 17th international conference on systems, signals and image processing (IWSSIP). 2010. p. 428–31.
[6] Iglesias JCA, Gomes ODM, Paciornik S. Automatic recognition of hematite grains under polarized reflected light microscopy through image analysis. Miner Eng 2011;24(12):1264–70.
[7] Gomes ODM, Iglesias JCA, Paciornik S, Vieira MB. Classification of hematite types in iron ores through circularly polarized light microscopy and image analysis. Miner Eng 2013;52:191–7.
[8] Durand LD, Iglesias JCA, Gomes ODM, Augusto KS, Domingues ALA, Paciornik S. Optimization of Image Acquisition for Hematite Classification in Iron Ores. In: SBMM organizer. Proceedings of 25th congress of Brazilian Society of Microscopy and Microanalysis. 2015.
[9] Delbem ID, Galéry R, Brandão PRG, Peres AEC. Semi-automated iron ore characterisation based on optical microscope analysis: quartz/resin classification. Miner Eng 2015;82:2–13.
[10] Donskoi E, Poliakov A, Manuel JR, Peterson M, Hapugoda S. Novel developments in optical image analysis for iron ore, sinter and coke characterisation. Appl Earth Sci 2015;124(4):227–44.
[11] Schindelin J, Arganda-Carreras I, Frise E, Kaynig V, Longair M, Pietzsch T, et al. Fiji: an open-source platform for biological-image analysis. Nat Methods 2012;9(7): 676–82.
[12] Eaton JW. Octave: past, present and future. In: Hornik K, Leisch F, editors. Proceedings of 2nd international workshop on distributed statistical computing. 2001.
[13] Sussman GJ, Steele GL. SCHEME: An interpreter for extended lambda calculus, AI Memo 349, CSAIL/MIT, Cambridge, Massachusetts, 1975. Reprinted in: Higher-Order and Symbolic Computation 1998; 11(4):405–39.
[14] JavaSIFT [homepage on the internet]. Saalfeld S, 2008 [cited 21.02.17]. Available from: http://fly.mpi-cbg.de/ saalfeld/Projects/javasift.html.
[15] Haralick RM, Shanmugam K, Dinstein I. Textural features for image classification. IEEE Trans Syst Man Cybern 1973;6:610–21.
[16] Canny J. A computational approach to edge detection. IEEE Trans Pattern Anal Mach Intell 1986;8(6):679–98.
[17] The LaTeX Project [homepage on the internet]. The LaTeX Team [cited 18.11.17]. Available from: https://www.latex-project.org/.